JOURNAL OF GEOPHYSICAL RESEARCH, VOL. 114, A10316, doi:10.1029/2009JA014399, 2009

Estimating *E* region density profiles from radio occultation measurements assisted by IDA4D

M. J. Nicolls,[1] F. S. Rodrigues,[2] G. S. Bust,[2] and J. L. Chau[3]

Received 27 April 2009; revised 13 July 2009; accepted 23 July 2009; published 23 October 2009.

[1] An alternative approach for estimating *E* region density profiles using radio occultation total electron content (ROTEC) measurements is presented. In this approach, the *F* region contribution to the measured ROTEC is removed using the estimated *F* region from an assimilative model of ionospheric density. *E* region density profiles are then obtained from a numerical inversion of the residual ROTEC, which is assumed to be the *E* region contribution to the ROTEC. The proposed technique has been applied to radio occultation measurements made by the Constellation Observing System for Meteorology, Ionosphere and Climate (COSMIC), while the *F* region specification is obtained from the Ionospheric Data Assimilation Four-Dimensional (IDA4D) algorithm. Examples of *E* region profiles obtained with this approach are presented and compared with nearby radar measurements at the magnetic equator. The results indicate that accurate estimates of the *E* region peak height and density can be obtained with this approach. This technique may be applicable to the estimation of *E* region conductivities with the global coverage provided by the radio occultation measurements.

Citation: Nicolls, M. J., F. S. Rodrigues, G. S. Bust, and J. L. Chau (2009), Estimating *E* region density profiles from radio occultation measurements assisted by IDA4D, *J. Geophys. Res.*, *114*, A10316, doi:10.1029/2009JA014399.

1. Introduction

[2] Radio occultation [e.g., *Phinney and Anderson*, 1968] is a remote sensing technique that has been used successfully to obtain global measurements of water vapor and temperature in the lower atmosphere [e.g., *Kursinski et al.*, 1996] and electron density in the ionosphere [e.g., *Hajj et al.*, 1994; *Hajj and Romans*, 1998; *Schreiner et al.*, 1999]. The technique utilizes differential phase measured by a low-Earth orbit (LEO) satellite that is tracking a setting or rising global positioning system (GPS) satellite. The inferred index of refraction through the Earth's ionosphere is a strong function of electron density. As a result, the integrated refractivity can be directly (linearly) related to the total electron content (TEC) using the excess phase measurements. Alternatively, bending angle measurements can be inverted to obtain vertical refractivity. For discussions of the different approaches, see *Schreiner et al.* [1999] and *Hajj et al.* [2002].

[3] A standard procedure to estimate profiles of electron density is to invert the radio occultation TEC (ROTEC) measurements using the so-called inverse Abel transform. This approach, however, assumes spherically symmetric density profiles wherever the occultation rays happen to pass through. Given the fact that the radio occultation geometry can often extend over tens of degrees of latitude and longitude, the spherical symmetry assumption is likely not to be met at low latitudes where large density gradients exist due to the development of the Appleton anomaly and other features. This necessary assumption is thought to be the major source of error in electron density estimates from the radio occultation method [e.g., *Schreiner et al.*, 1999; *Garcia-Fernandez et al.*, 2003; *Wu et al.*, 2009a]. Nevertheless, on the average and when interpreted correctly, occultation-based measurements of the ionospheric *F* region reproduce expected variations and allow for global studies of large-scale ionospheric features [e.g., *Hajj and Romans*, 1998; *Schreiner et al.*, 1999; *Jakowski et al.*, 2002; *Lei et al.*, 2007].

[4] Several studies have focussed on improving inversions of radio occultation measurements using some kind of additional information. The added measurements are included in order to mitigate the effects of *F* region gradients in electron density [e.g., *Hajj et al.*, 1994]. Most studies have used slant or vertical TEC measurements from ground-based dual-frequency GPS receivers or *F* region peak density measurements from ionosondes to constrain the inversion problem [e.g., *Hajj and Romans*, 1998; *Schreiner et al.*, 1999; *Hernandez-Pajares et al.*, 2000; *Garcia-Fernandez et al.*, 2003; *Tsai and Tsai*, 2004; *Wu et al.*, 2008]. Other methods focus on correcting the inverted densities using properties of the induced asymmetry caused by horizontal gradients [*Straus*, 1999; *Wu et al.*, 2009b]. While these various studies have focussed on the *F* region, fewer investigations have focussed on the estimation of the densities at *E* region heights. *Mayer and Jakowski* [2009]

[1]Center for Geospace Studies, SRI International, Menlo Park, California, USA.
[2]Atmospheric & Space Technology Research Associates, San Antonio, Texas, USA.
[3]Radio Observatorio de Jicamarca, Instituto Geofisico del Peru, Lima, Peru.

0148-0227/09/2009JA014399$09.00

have investigated densities associated with particle precipitation in the auroral region by focussing on profiles dominated by the *E* region (typically nighttime in the auroral zone). Some studies [e.g., *Straus*, 1999; *Hysell*, 2007; R. L. Bishop et al., personal communication, 2008] have investigated improved inversion algorithms useful for identifying localized *E* region features. In addition, radio occultation measurements have already proven quite useful in investigating global sporadic *E* morphology [*Wu et al.*, 2005b].

[5] It is believed that LEO-GPS occultation measurements can provide a global database of *E* region densities and derived conductivities given an adequate/robust technique for the inversion of *E* region density profiles. Near the magnetic equator, measurements of *E* region densities are important for quantitative analysis of the equatorial electrojet [e.g., *Forbes*, 1981] and associated phenomena [e.g., *Martinis et al.*, 2003; *Shume et al.*, 2005b; *Dyrud et al.*, 2007]. Measurements near sunset and sunrise could lead to a better understanding of the role of *E* region effects on the day-to-day variability and seeding of equatorial spread *F* (ESF) [e.g., *Kelley et al.*, 2004], which is a major source of space weather at low latitudes. *E* region conductivities influence the electrodynamics near the magnetic equator, playing an important role in determining the conditions conducive for instability (for example, the magnitude of the prereversal enhancement [e.g., *Fesen et al.*, 2000]) and the growth rates themselves, both directly [e.g., *Zalesak and Ossakow*, 1982; *Sultan*, 1996; *Hysell and Kudeki*, 2004], and indirectly, by gradients in the off-equatorial Hall conductivity and perhaps by polarization electric fields in off-equatorial sporadic *E* layers [e.g., *Tsunoda*, 2006].

[6] Measurements of lower ionospheric electron densities have typically been confined to single-location ground-based measurements, such as with the incoherent scatter (IS) technique at the Jicamarca Radio Observatory [*Chau and Woodman*, 2005], which uses measurements associated with thermal backscatter to infer the electron density. Jicamarca IS radar measurements of the *D* and *E* region, however, are limited to daytime and periods when the electrojet is not present. Additionally, equatorial *E* region densities have also being inferred from the Faraday rotation of coherently scattered echoes [*Hysell and Chau*, 2001; *Shume et al.*, 2005a]. Ionosonde measurements, such as those from a digital portable sounder (DPS) [*Reinisch*, 1986], are able to measure the peak density and altitude of the *E* region and infer bottomside and topside profiles with some assumptions. The other main database of lower ionospheric densities comes from a radio wave propagation experiment with rocket soundings, subsequently used to formulate the Faraday-IRI (FIRI) model [*Friedrich and Torkar*, 2001], a correction to the International Reference Ionosphere (IRI) [*Bilitza*, 2001] in the *D* and *E* regions.

[7] In this report, we present a new method to estimate *E* region density profiles from radio occultation measurements. This method is applied to occultation measurements made by the Constellation Observing System for Meteorology, Climate, and Ionosphere (COSMIC) using the Ionospheric Data Assimilation Four-Dimensional (IDA4D) algorithm. In section 2, details about the inversion method are given as well as details about COSMIC and IDA4D. Section 3 presents examples of the inverted *E* region density profiles. The results are compared with profiles measured by a ground-based bistatic radar located near the geomagnetic equator and profiles predicted by IRI and FIRI. The main conclusions are summarized in section 4.

2. Methodology and Data

2.1. Radio Occultation TEC

[8] Radio occultation measurements provide excess phase observables on two L band frequencies, L1 (f_1 = 1.57542 GHz) and L2 (f_2 = 1.22760 GHz). The excess phase can be converted to radio occultation TEC (ROTEC) given the relationship between the integrated refractive index and the integrated electron density prescribed by the Appleton-Hartree equation [e.g., *Hajj et al.*, 2000]. The desired straight-line TEC can be computed using a classical approach that involves differencing the excess phase measurements on L1 and L2, which has the benefit of removing errors associated with transmitter and receiver clock uncertainties and orbital information, at the expense of additional random noise [e.g., *Schreiner et al.*, 1999; *Hajj et al.*, 2000; *Syndergaard*, 2002]. Alternatively, using precise orbital information, ROTEC can be computed on a single frequency using a more accurate differencing technique that essentially eliminates errors associated with bending and dispersion [*Syndergaard*, 2002]. This approach has the form

$$\mathrm{TEC} = \frac{f_2^4 L_2 - f_1^4 L_1}{C(f_1^2 - f_2^2)} \tag{1}$$

where L_1 and L_2 (units of meters) are the excess phase measurements on f_1 and f_2, respectively, and C = 40.3082 m^3/s^2. The resulting residuals are associated with a term due to the presence of the geomagnetic field in the Appleton-Hartree equation, although errors associated with the LEO velocity are in general larger [*Syndergaard*, 2002]. The total system error is then $\sim$1–2 TECU (1 TECU = 10^{16} electrons/m^2) [*Syndergaard*, 2002]. It is this approach that is used for the ROTEC measurements in this paper.

[9] Thus, radio occultation measurements provide the TEC along the raypath between a LEO satellite and a GPS satellite as a function of the height of the tangent point (h_{tp}) of the path (referred to as ROTEC). Because both LEO and GPS satellites are moving at high speeds, the location of the tangent point can vary several degrees in latitude and longitude while the tangent point varies over a few hundreds of kilometers at *E* and *F* region altitudes. Therefore, each occultation ray can pass through *E* and *F* regions at different locations and with significantly different ionospheres. This ''smearing'' is particularly important at low latitudes and Figure 1 illustrates the case for an occultation over South America on 5 April 2007.

[10] Figure 1a shows the coordinates of various occultation rays (blue lines), and the coordinate of the tangent points (points perpendicular to rays), overplotted on the vertical TEC predicted by IDA4D (to be discussed later). The location where the height of the occultation ray is between 80 and 150 km is shown in red. Large horizontal gradients in the vertical TEC can be observed around the occultation region. These gradients correspond to *F* region density gradients associated with the low-latitude anomaly region.

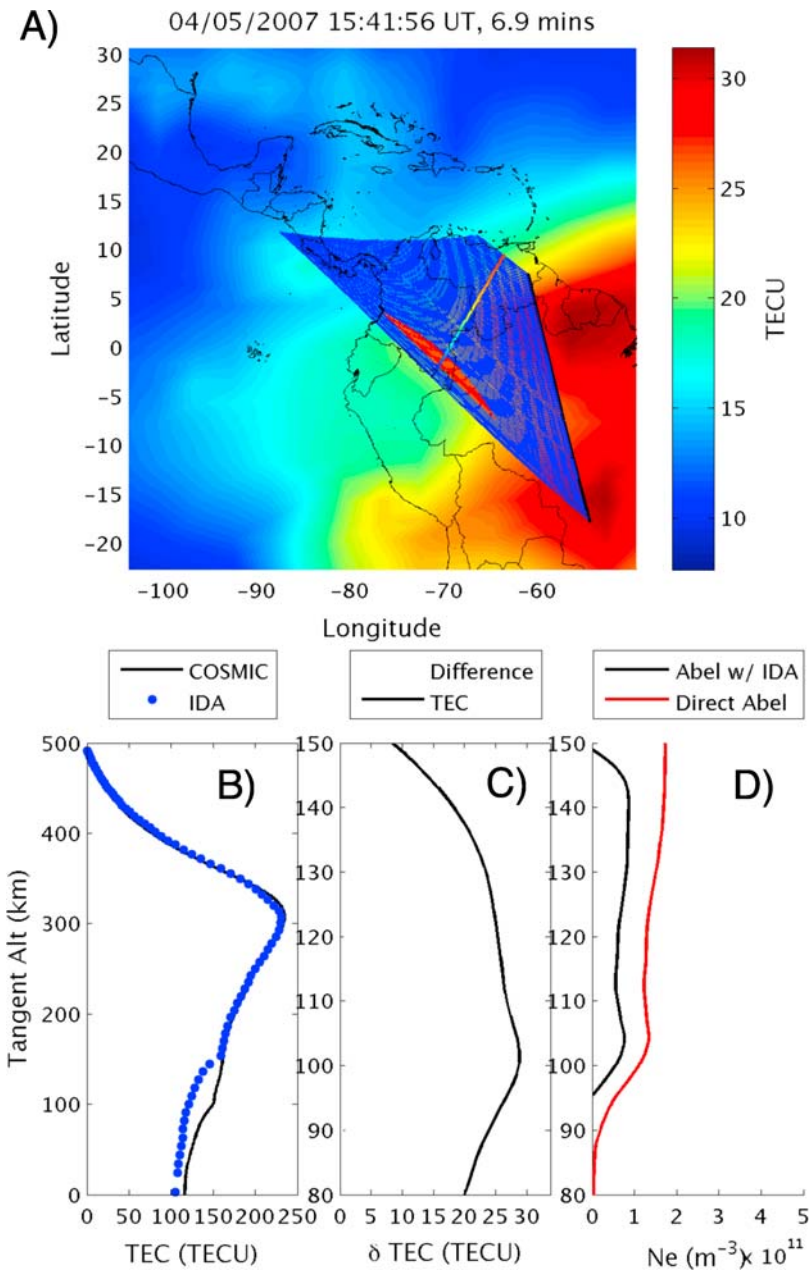

Figure 1. Radio occultation measurement between COSMIC satellite 3 and GPS satellite 24 at ~1541 UT on 5 April 2007. (a) Occultation geometry overlaid on IDA vertical TEC as a function of latitude and longitude. Black dots show the projection of the LEO satellite position, blue lines show occultation rays to the GPS satellite, and colored lines perpendicular to the rays show the position of the tangent points. Red colored lines indicate where rays lie between 80 and 150 km. Longer rays penetrate deeper into the ionosphere with correspondingly lower tangent altitudes. (b) COSMIC ROTEC (black) and TEC predicted by IDA (blue dots) along the occultation path (altitudes above 150 km). (c) Difference in IDA and ROTEC, corresponding to contribution below 150 km. (d) N_e determined from an Abel inverse transform of the difference TEC (black) and from a direct Abel inversion of the occultation TEC (red).

[11] The ROTEC measured along occultations (see Figure 1b) with tangent heights below ~110 km has contributions from electron densities in the *E* and *F* regions. Therefore, it can be stated that the measured ROTEC for these raypaths is a sum of the TEC along the raypath going through *E* region (*E* region ROTEC) and *F* region (*F* region ROTEC) heights. Because the peak density in the *F* region can be ten or more times larger than the *E* region peak density with significantly larger scale heights, and because the raypath in the *F* region is usually longer than the path through the *E* region, the *F* region ROTEC is, in general, much larger than the *E* region ROTEC. Nevertheless, the *E* region ROTEC is significant, especially during the day and cannot be ignored, in particular on those rays that have

tangent points (longest part of the ray) through the *E* region. In addition, the occurrence of *E* region sporadic layers can significantly increase the *E* region contribution to the total occultation TEC.

2.2. Approach for Estimation of *E* Region Density Profiles

[12] In order to estimate *E* region density profiles, we propose an accurate removal of the *F* region ROTEC from the total (measured) ROTEC. *E* region density profiles are then estimated from the resulting *E* region ROTEC. Accurate estimation of *F* region ROTEC is obtained from the results of an assimilative model of ionospheric densities. For this study, we used the Ionospheric Data Assimilation Four-Dimensional (IDA4D) algorithm. More details about this algorithm are given in section 2.4.

[13] Once the *E* region ROTEC is obtained, the *E* region density profiles can be estimated using the standard inverse Abel transform:

$$N_e(r) = -\frac{1}{\pi}\int_r^\infty \frac{dTEC/ds}{\sqrt{s^2 - r^2}}\,ds \qquad (2)$$

where r is radial distance from the center of the Earth, s is the tangent altitude, and $dTEC/ds$ is the derivative of the residual ROTEC with respect to the tangent altitude. This approach does not require absolute removal of any TEC biases, as it relies only on the gradient of the ROTEC. Note also that spherical symmetry is a condition more likely to be met in the *E* region, as we will show and discuss later.

2.3. COSMIC

[14] The methodology described in section 2.2 was applied to radio occultation measurements made by the GPS radio occultation experiment on board COSMIC satellites. COSMIC is the Constellation Observing System for Meteorology, Ionosphere and Climate and Taiwan's third Formosa Satellite Mission (FORMOSAT-3). The COSMIC/FORMOSAT-3 mission is a joint scientific project between Taiwan and the US [e.g., *Wu et al.*, 2005a; *Liou et al.*, 2007; *Anthes et al.*, 2008], with the objective to collect atmospheric data for weather prediction and for ionosphere, climate, and gravity research. The COSMIC constellation includes six LEO microsatellites launched on 15 April 2006 from Vandenberg AFB, CA. The satellites were launched into the same circular, 72 inclination orbit at an altitude of 512 km. The satellites then moved into six different orbital planes. It is expected that the satellites will reach a final altitude of about 800 km within 5 years of the launch. Each satellite has three scientific payloads on board: a tiny ionospheric photometer (TIP) for measurements of night sky airglow emissions, a triband beacon (TBB) transmitting phase coherent signals at three different frequencies, and a GPS receiver for radio occultation experiments (GOX). The GPS receivers are the primary payload of the COSMIC satellites and their observations are used in this study.

2.4. IDA4D

[15] The Ionospheric Data Assimilation Four-Dimensional (IDA4D) is an assimilative algorithm for four-dimensional (latitude, longitude, altitude, and time) imaging of ionospheric densities [*Bust et al.*, 2004, 2007]. IDA4D is an objective analysis maximum likelihood algorithm that makes use of a background model ionosphere, model error covariance, and data error covariance. It is based on three-dimensional variation (3DVAR) data assimilation [*Daley*, 1991; *Daley and Barker*, 2000]. IDA4D is able to ingest a large number of different data sources, including ground-based GPS TEC, beacon TEC data from low-Earth orbiting (LEO) satellites, satellite-based GPS occultation data, and satellite-based TEC data from the onboard GPS navigation receiver (the so-called Over Satellite Electron Content data). IDA4D can also accept point measurements of electron density from a number of instruments including incoherent scatter radars and ionosondes, and satellite in situ measurements, for example, from Defense Meteorological Satellites Program (DMSP) or the Challenging Minisatellite Payload (CHAMP). In addition, IDA4D can ingest various types of observations nonlinearly related to electron density including ionosonde virtual height versus frequency data, oblique HF sounder data, and EUV observations from sensors such as the Global Ultraviolet Imager (GUVI) and TIP.

[16] For this study, IDA4D assimilated observations made by ionosondes, ground-based GPS TEC, GUVI radiances, DORIS, CHAMP and GRACE occultations. Note, however, that the digisonde located at Jicamarca, Peru was specifically not ingested so as to construct a meaningful and fair validation/comparison exercise. To optimize data usage and to improve the *F* region density specification, IDA4D also assimilated COSMIC occultations with tangent heights above 150-km altitude. The *E* region inversion is applied only to occultations measurements with tangent heights below 150-km altitude. The Advanced Space Environment (ASPEN) version of the Thermosphere Ionosphere Mesosphere General Circulation Model (TIMEGCM) [*Roble and Ridley*, 1994] was used as the background model. IDA4D was set up to provide electron density estimates from 50 km up to 2000 km altitude every 15 minutes in a global grid with resolution of about 4 latitude and 9 longitude over South America. The grid has better resolution in regions where a larger number of measurements are being assimilated (in the US for instance, where a large network of GPS TEC receivers is available). The height resolution varied between 20 km in the main *F* region and 100 km above 1000 km altitude.

2.5. Validation

[17] We focus our analysis on occultations occurring near the geomagnetic equator and over (or close to) South America. The equatorial *E* region in general does not exhibit the same layering found in the off-equatorial low-latitude regions where sporadic layers can develop, and thus we choose to validate in this region where strong altitudinal and horizontal gradients in the *E* region densities are not expected. In addition, this region is of great scientific interest due to *E* region effects on current systems and the development of convective ionospheric storms [e.g., *Kelley et al.*, 2004].

[18] Despite the scientific interest and importance of the equatorial *E* region, only recently has a capability been developed for obtaining *E* region density profiles at the magnetic equator [*Hysell and Chau*, 2001; *Shume et al.*, 2005a]. This is mostly because the magnetic equator is in general a region inaccessible to incoherent scatter radars due

to clutter from electrojet irregularities [*Chau and Woodman*, 2005]. The method developed by [*Hysell and Chau*, 2001] and refined by [*Shume et al.*, 2005a] uses a bistatic coherent scatter radar system with a transmitter located at Jicamarca, Peru (11.95°S, 76.87°W), and a receiver located at Paracas, Peru (13.85°S, 76.25°W), and takes advantage of the Faraday rotation of the coherently scattered signal to infer densities through the *E* region. These measurements have an altitude resolution of better than a kilometer and relative uncertainties of less than one percent [*Shume et al.*, 2005a].

[19] In order to investigate the validity of the IDA4D-assisted inversions, we compare the inverted *E* region profiles with *E* region profiles measured by the Jicamarca-Paracas radar. Additionally, we compare the results of our inversions with the International Reference Ionosphere (IRI) [*Bilitza*, 2001] and FIRI [*Friedrich and Torkar*, 2001]. FIRI (an optional input to the IRI2007 model) is an empirical correction to the *D* and *E* region electron densities in IRI based on rocket sounding measurements and has been shown to be in better agreement with equatorial electron densities [e.g., *Shume et al.*, 2005b]. The radar measurements are usually limited to altitudes between 95 and 110 km. Comparing our results with standard ionospheric models can give us some insight on the quality of the inversions at altitudes below and above the radar measurements. Also, this comparison gives us another opportunity to investigate how model predictions compare with the Jicamarca radar measurements.

3. Results and Discussion

3.1. IDA4D *F* Region ROTEC

[20] Figure 1a illustrates the fact that any attempt to infer electron densities in the *E* region (red lines) will be strongly affected by electron density gradients in the *F* region. Rays that pass through the *E* region have asymmetric contributions from the *F* region portions of the rays, with a gradient in the vertical TEC (as predicted by IDA) of over 20 TECU. By subtracting *F* region electron density estimates from IDA4D, we effectively remove any effects of *F* region horizontal gradients along the occultation raypaths.

[21] Figure 1b shows COSMIC ROTEC (solid black curve) and the *F* region ROTEC predicted by IDA (blue dots). It can be seen that IDA4D reproduces very well the ROTEC down to 150-km tangent altitude. The *F* region portions of the ROTEC agree to within ~3.5–4 TECU (root-mean-square) from 150–500 km tangent altitudes. This excellent agreement is due, at least in part, to the fact that we have ingested the *F* region portion of the occultations into IDA4D in addition to other measurements available. A good forecast specification also contributes to the accuracy of the IDA4D density estimate. We can make the reasonable conjecture that with this good agreement, and with a reasonable estimate of *F* region correlation lengths, IDA4D can construct and provide reliable estimates of the *F* region contribution to the measured *E* region ROTEC.

[22] Figure 1c shows the subtracted, or difference TEC, which is the expected contribution from the *E* region. Note that it is the gradient of this TEC that is used to infer the electron density via the inverse Abel transform. The resulting density profile for this particular occultation is shown in Figure 1d (black). The estimated density that would be obtained via a direct inversion of the ROTEC neglecting *F* region gradients is shown in red. Including the *F* region gradient specification from IDA4D in general reduces the magnitude of the *E* region N_e. This difference in the two methods is most pronounced on the bottomside where the resultant profile shows that the *E* region N_e has been reduced to a negligible value by 95 km; the direct ROTEC profile, on the other hand, shows high densities down to below 90 km.

3.2. Occultation Measurements Near Jicamarca

[23] As mentioned earlier, we focus on occultations near the magnetic equator over South America, more specifically around Jicamarca where radar measurements of *E* region density profiles are available (see section 2). The results presented in this report are for 1, 5, and 15 April 2007. The Jicamarca-Paracas bistatic radar system was able to make continuous measurements of the *E* region for 6 hours or more on these days. The measurements are limited to daytime only (usually between 0800 LT and 1600 LT) when electrojet irregularities are present to cause the radio wave scattering necessary for the radar observations. The geometry of daytime occultations occurring close to Jicamarca for these three days is shown in Figure 2. Only the projection of the rays passing through the region 80–150 km has been plotted (red lines), along with the locations of the tangent points (black points). The location of the Jicamarca and Paracas radar sites are also shown (blue dots).

[24] Figure 2 illustrates how difficult it is to find an occultation over a specific location. This makes a direct comparison between occultation measurements and ground-based measurements somewhat difficult. The occultation rays passing through *E* region heights usually cover many degrees in latitude and longitude as shown in Figure 2, although we remind the reader that the most of the contribution to the integrated *E* region ROTEC comes from densities at or near the tangent point.

[25] The occultation measurements whose geometries are shown in Figure 2 were used to estimate *E* region density profiles using our approach (section 2.2). Next, we present and discuss how the inverted profiles compare with the *E* region measurements made by the Jicamarca-Paracas radar system and with predictions made by the IRI and FIRI.

3.3. Comparison Between Measurements and Model Predictions

[26] Figure 3 (left) shows an example of the inverted profiles using the proposed ROTEC/IDA4D approach for the same occultation presented in Figure 1. The occultation-based result is shown in red, Jicamarca measurements as blue points, and IRI and FIRI as black dashed and dashed-dotted lines, respectively. Overall, the inverted profile is in good agreement with the profile measured by the radar. We note that the distance of this occultation (from the tangent point at 100-km altitude) to the radar site was approximately 1300 km. Despite this nonnegligible separation distance, the peak density and height from the occultation is in excellent agreement with the peak height (h_mE) and density (N_mE) measured by the bistatic radar.

[27] A second profile on 5 April is shown in Figure 3 (right). Again, the inverted profile agrees well with the Jicamarca N_mE and h_mE. On the bottomside, however, the

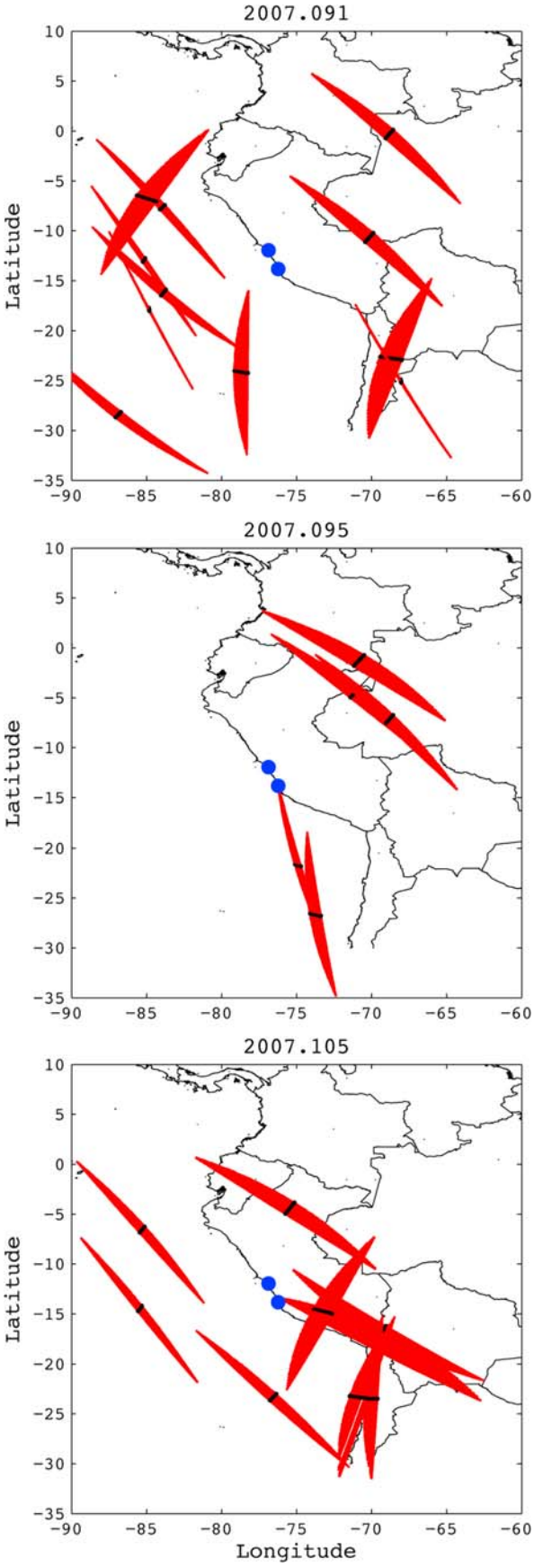

measurements show a smaller E region scale height than the RO/IDA4D estimates. This bottomside scale height is in good agreement with the standard IRI-predicted scale height and likely denotes a slight misestimation of the horizontal F region gradients.

[28] As we will show next, we also found that FIRI is in better agreement with the radar measurements than IRI. Both IRI and FIRI predict similar N_mE and h_mE values but IRI tends to overestimate the density in the lower E region. The scale height difference between the standard IRI and the bistatic radar N_e has been pointed out before and discussed extensively by *Hysell and Chau* [2001] and *Shume et al.* [2005a]. *Shume et al.* [2005a] showed that the shape of the E region density profiles measured by the radar agree well with an α-Chapman function with N_mE and h_mE estimated from IRI. *Shume et al.* [2005b] also pointed out that FIRI predictions are in better agreement with the radar measurements. However, recent rocket and ALTAIR-radar measurements near the magnetic equator by *Friedrich et al.* [2006] showed excellent agreement with IRI from ~85–100 km and excellent agreement with FIRI from ~60–80 km.

[29] To illustrate the consistency of IDA4D F region specification and of the inverted E region profiles, similar profile comparisons are shown in Figure 4 and Figure 5 for 1 and 15 April 2007, respectively. These profiles represent typical inversion results. On 1 April, all three profiles show good agreement with the Jicamarca density scale height and peak, but a small underestimation of the peak density. In the third profile, at ~21 UT, the occultation measurements show a much smaller E region peak than FIRI or standard IRI. The radar measurements, unfortunately, do not extend to above 100 km (they require the presence of reasonably strong coherent echoes from the electrojet) but below 100 km the ROTEC N_e agrees well with the measurements. On 15 April, for the three profiles shown, the peak densities and scales are in good agreement with the radar measurements. In general, the occultation profiles show similar features to the radar measurements and to FIRI, although the measurements often fall between FIRI and IRI.

[30] These results suggest that the overall mean features of the equatorial E region are captured in the inversions. The results shown in Figures 3, 4, and 5 indicate that the inverted densities between 95 and 110 km agree reasonably well with densities measured by the Jicamarca-Paracas radar system. One must keep in mind that the inversion approach assumes spherical symmetry for the E region probed by the occultations. The E region at low latitudes can be considered less dynamic than its midlatitude counterpart. The long occultation raypaths (see Figure 2), however, can probe E regions being illuminated at different solar zenith angles and can be significantly different in some cases. This can explain, at least in part, the differences between the inverted profiles and the profiles measured by the radar or predicted by FIRI.

Figure 2. Occultation geometry for occultations close to Jicamarca/Paracas on (top) 1 April, (middle) 5 April, and (bottom) 15 April 2007. Red lines indicated raypaths between the altitudes of 80–150 km, black dots are tangent altitudes, and blue dots are Jicamarca and Paracas locations.

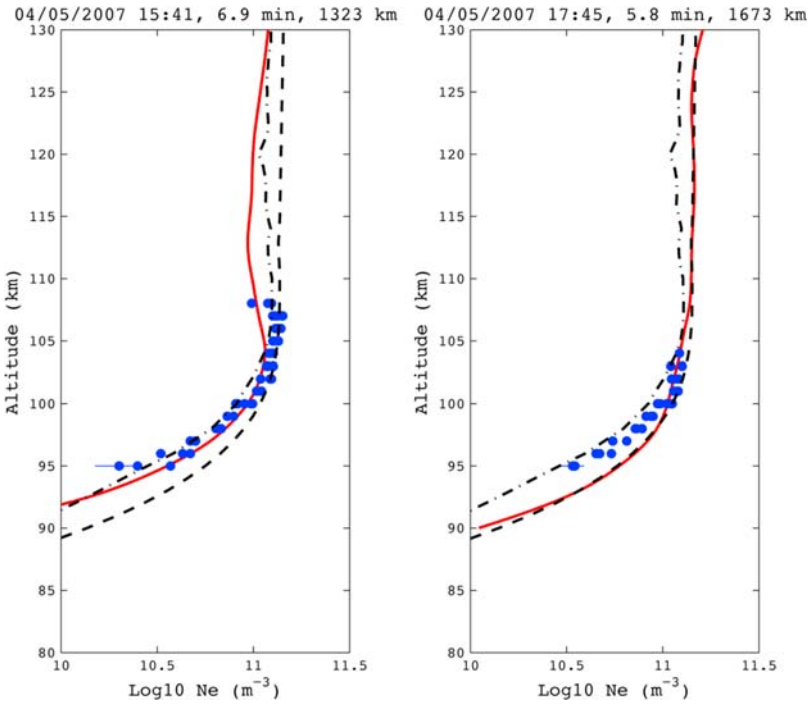

Figure 3. Comparison of occultation-based N_e (red), IRI N_e (black dashed), FIRI N_e (black dashed-dotted), and Jicamarca-Paracas bistatic N_e (blue points) at two times (~1541 and ~1745 UT). Error bars on the radar N_e estimates are not plotted since they are smaller than the variability of the data; thus, we have also plotted points for the profiles before and after the time of interest. The title bar indicates the occultation time, duration, and distance from Jicamarca at an altitude of 100 km.

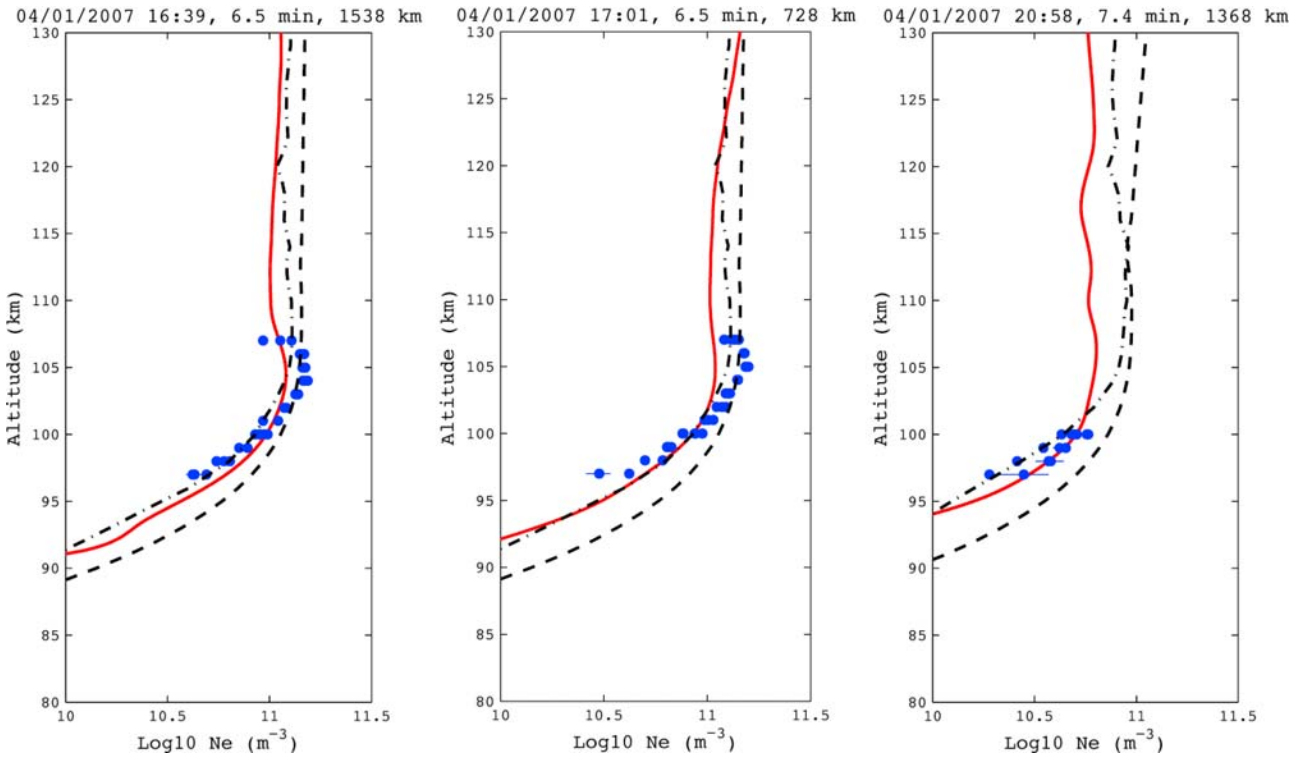

Figure 4. Same as Figure 3 for three occultations on 1 April 2007.

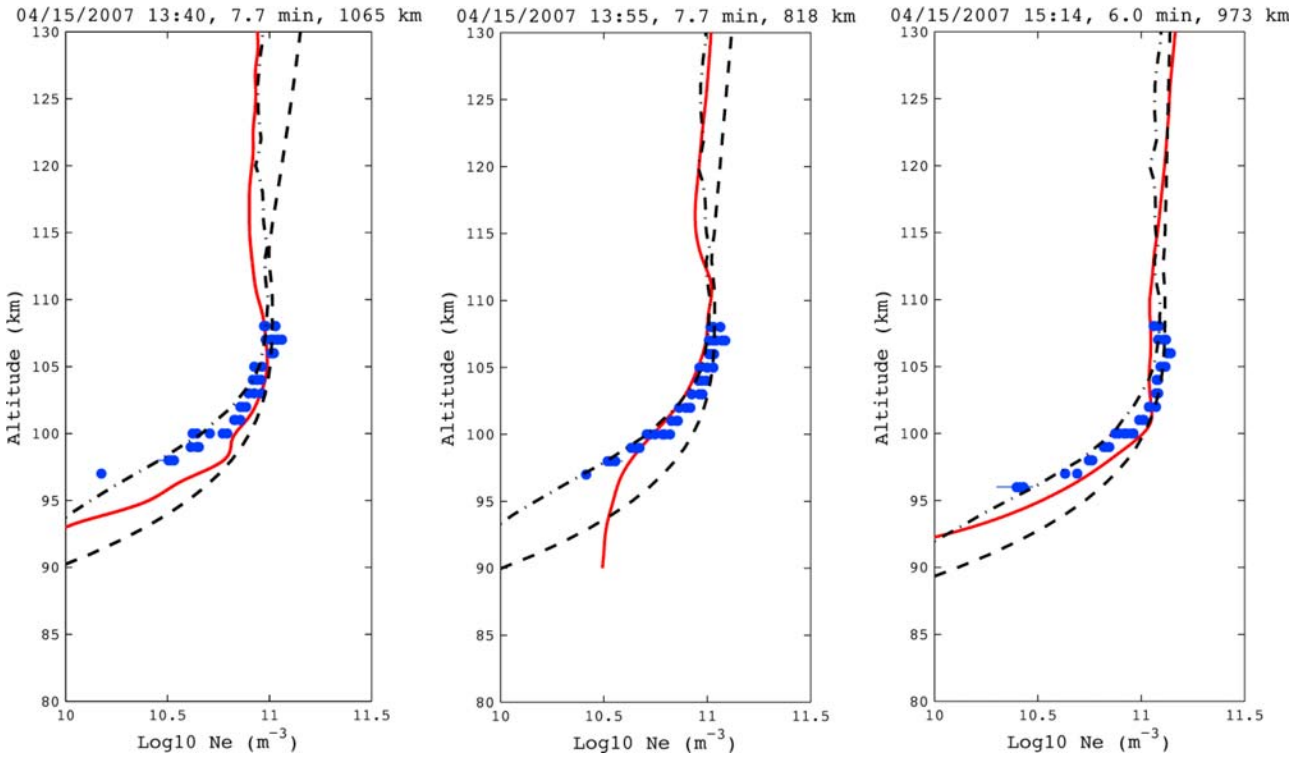

Figure 5. Same as Figure 3 for three occultations on 15 April 2007.

[31] In order to illustrate the long correlation lengths at *E* region heights and to justify our spherical symmetry assumption for the *E* region, Figure 6 shows the spatial variation of N_mE over South America predicted by FIRI. While a physics-based model would be more realistic, IRI does include an accurate measure of the expected density gradients due to typical solar zenith angle induced differences in ionization rates. Predictions for 1400, 1630, and 1900 UT are shown. One can see that the correlation lengths are several degrees in both latitude and longitude and that spherical symmetry is a reasonable assumption for the typical horizontal distances probed by occultations.

3.4. Solar Zenith Angle Dependence

[32] Section 3.3 showed a direct comparison of a few typical inverted density profiles with independent ground-based measurements and predictions by standard ionospheric models. Figures 7, 8, and 9 show comparisons of the electron densities at three altitudes (100, 105, and 110 km) as a function of time for 1, 5, and 15 April, respectively. Note that local time in Peru is UT-5 hours (local noon is 1700 UT). These comparisons show results covering a larger number of occultation measurements and serve to investigate whether the inverted profiles are accurate enough to provide information on changes due to geophysical conditions, namely the *E* region solar zenith angle dependence. All occultations in reasonable proximity to the Jicamarca-Paracas bistatic radar (see Figure 2) have been shown. The *E* region is mainly produced by solar UV (photoionization of O_2, N_2, and O) and therefore the electron density has a strong solar zenith angle dependence. This effect, more clear in the decreasing density especially at the lower altitudes, is evident in the radar measurements and in the occultation profiles (see, for example, Figure 7).

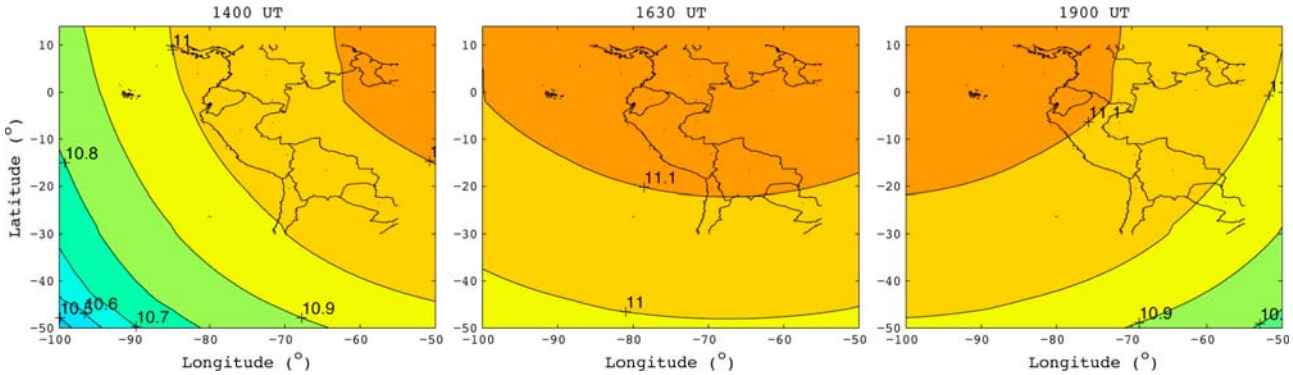

Figure 6. Log10 of N_mE predicted by FIRI on 15 April 2007 at 1400 UT, 1630 UT, and 1900 UT.

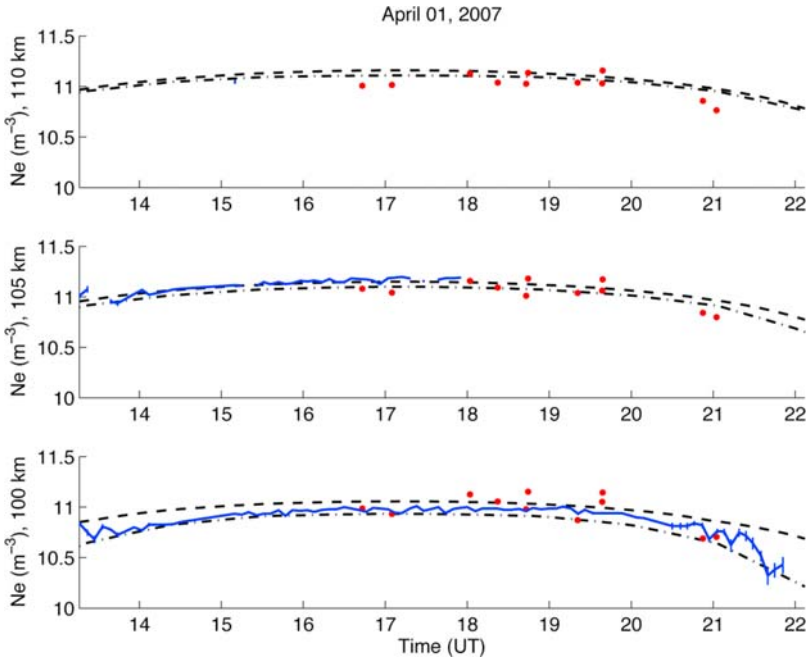

Figure 7. Log of electron density at (bottom) 100 km, (middle) 105 km, and (top) 110 km from Jicamarca (blue), IRI (black dashed), FIRI (black dashed-dotted), and the occultation inversions (red dots) on 1 April 2007.

[33] This comparison again shows good agreement between FIRI, IRI and the radar measurements at altitudes around the *E* region peak (say between 105–110 km). Note that the radar observations typically can not provide density values for altitudes above 110 km. As shown earlier, IRI overestimates the daytime densities at lower altitudes (say 100 km). In general, the radar measurements tend to lie between the values predicted by IRI and FIRI. While there is some variability in the results, one can see good agreement between the occultation densities and the radar N_e for virtually all data points. The solar zenith angle effects can also be seen in the occultation measurements whenever data measurements are available early in the day or late in the afternoon. This suggests that the IDA4D-assisted inversion of ROTEC measurements are sufficiently accurate to resolve altitude profiles in the daytime *E* region.

[34] Absolute errors on the inverted densities are difficult to estimate because most of the uncertainty is expected to be

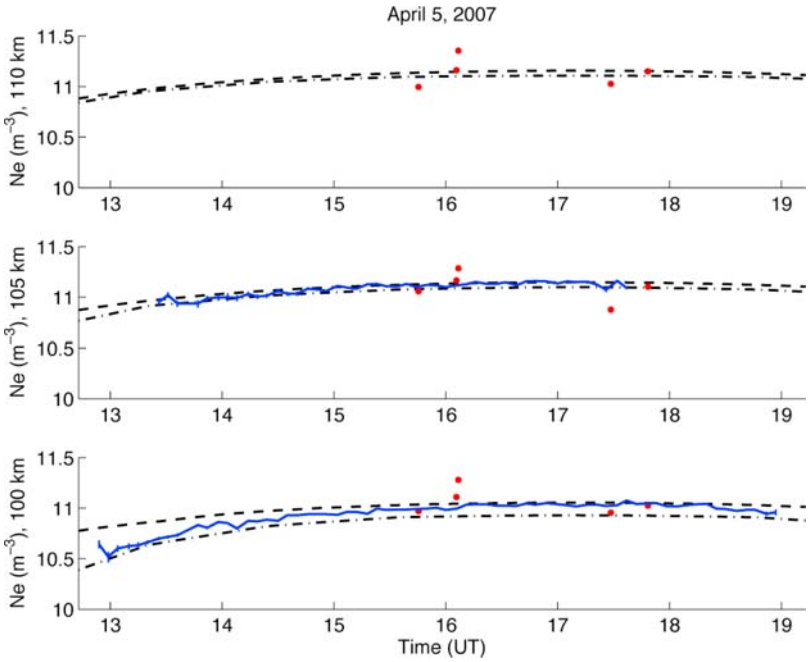

Figure 8. Same as Figure 7 for 5 April 2007.

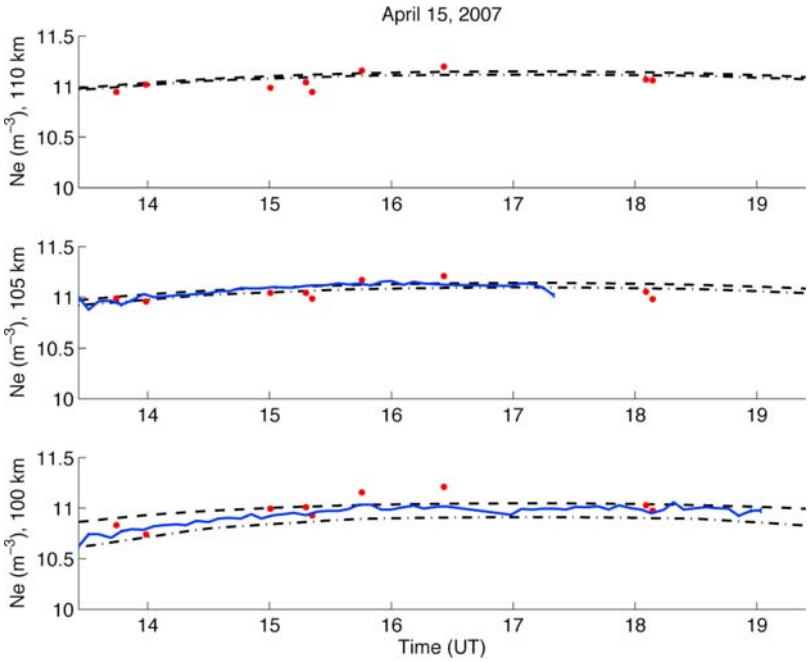

Figure 9. Same as Figure 7 for 15 April 2007.

due to unknown biases in the difference ROTEC caused by a number of sources. However, treating the Jicamarca-Paracas measurements as ground truth, the differences in the estimated densities and the densities measured by the radar can be representative of the expected errors (see Figures 7, 8, and 9). In Figure 10, we show histograms of the root-mean-square density differences (left), the root-mean-square fractional differences (middle), and a scatterplot of the density as a function of the distance from the radar (right) for each occultation profile used in Figures 7, 8, and 9. The root-mean-square errors for a given profile were computed using all altitudes where both Jicamarca radar data and occultations were available. The root-mean-square errors are typically around $1-2 \times 10^{10}$ m^{-3}, corresponding to fractional errors of about 20–25%. Figure 10 (right) shows that indeed there is a tendency for distant occultations to have larger root-mean-square errors, implying that at least some of the variability is geophysical in nature.

4. Conclusions

[35] We have presented an alternative approach for the inversion of *E* region density profiles from radio occultation measurements. This method uses densities estimated by an assimilative model of the ionosphere to estimate the *F*

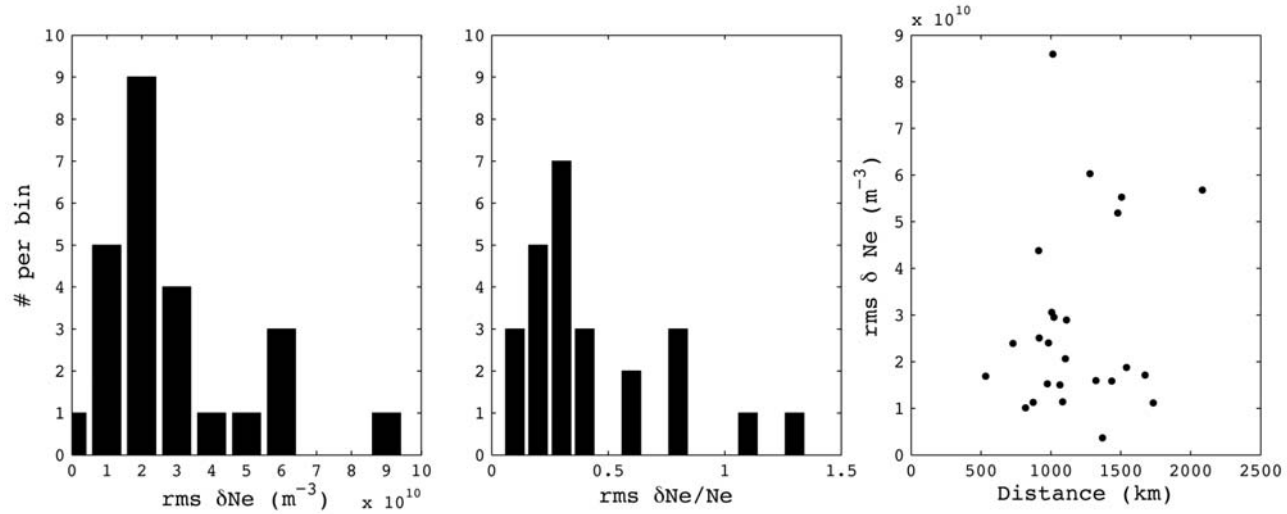

Figure 10. (left) Histogram of root-mean-square errors (bin size of 1×10^{10} m^{-3}) using Jicamarca as ground truth for occultation profiles on all three days. (middle) Histogram of fractional root-mean-square errors (bin size of 0.1). (right) Scatterplot of root mean square error as a function of the distance of the occultation (at 100 km altitude) to Jicamarca.

region contribution to the total ROTEC measurements. Once the F region contribution is removed from the measured ROTEC, we assume the remaining ROTEC is representative of electron densities at E region heights. We also assume that the E region does not vary much in the region probed by the occultation measurement (that the assumption of spherical symmetry is valid). E region density profiles are estimated from the E region ROTEC using the inverse Abel transform. Ionospheric model predictions and inverted results indicate that our assumptions are reasonable.

[36] We applied this approach to radio occultation measurements made by COSMIC with F region densities were specified by IDA4D. We point out, however, that the proposed approach can use results from other assimilative ionospheric models and occultation measurements made by other satellites. Results showing that IDA4D reproduces the F region gradients observed at low latitudes and the observed F region ROTEC were presented. We compared the inverted E region profiles with density profiles measured using the Faraday rotation technique by a bistatic coherent scatter radar system near the Jicamarca Radio Observatory. We found that the inverted profiles are in good agreement with radar profiles. As expected, small differences between radar measurements and inversions are observed at some times and altitudes. These differences can be caused by a number of reasons, including (1) inaccuracies in the IDA4D F region specification, (2) spatial gradients in the E region probed by the radio occultation raypaths caused, for instance, by differences in the solar zenith angle along the path, (3) density gradients at plasmaspheric heights, and (4) inaccuracies in the measured ROTEC. The differences in the estimated densities and densities measured by the radar can be representative of the expected errors (see Figure 10). These errors, however, seem to be small enough ($\sim 2 \times 10^{10}$ m^{-3}) that we are able to identify changes in the geophysical conditions such as the solar zenith control of the daytime densities.

[37] We also presented comparisons of our inverted profiles with profiles predicted by IRI and FIRI. As shown by *Shume et al.* [2005a, 2005b], IRI tends to overestimate the densities in the lower E region when compared with the radar measurements. On the other hand, FIRI seems to agree well with the radar measurements. In particular, N_mE and h_mE values are usually in good agreement between IRI, FIRI, radar measurements and our E region estimates.

[38] Future work will include comparisons of profiles obtained using the proposed ROTEC-IDA4D approach with midlatitude E region measurements made by the Arecibo IS radar. We will also attempt to take advantage of the global coverage of the occultation measurements to obtain longitudinal and latitudinal profiles of daytime E region densities to investigate the role of the E region on the electrodynamics of the low-latitude and equatorial region.

[39] **Acknowledgments.** Research at SRI International and ASTRA was funded by NSF award ATM-0719808. The Jicamarca Radio Observatory is a facility of the Instituto Geofisico del Perú operated with support from the NSF Cooperative Agreement ATM-0432565 through Cornell University. The authors would like to acknowledge Seebany Datta-Barua for comments on a draft of this manuscript.

[40] Amitava Bhattacharjee thanks Martin Friedrich and another reviewer for their assistance in evaluating this paper.

References

Anthes, R. A., et al. (2008), The COSMIC/FORMOSAT-3 mission: Early results, *Bull. Am. Meteorol. Soc.*, *89*, 313–333, doi:10.1175/BAMS-89-3-313.

Bilitza, D. (2001), International Reference Ionosphere 2000, *Radio Sci.*, *36*(2), 261–275.

Bust, G. S., T. W. Garner, and T. L. Gaussiran II (2004), Ionospheric Data Assimilation Three-Dimensional (IDA3D): A global, multisensor, electron density specification algorithm, *J. Geophys. Res.*, *109*, A11312, doi:10.1029/2003JA010234.

Bust, G. S., G. Crowley, T. W. Garner, T. L. Gaussiran II, R. W. Meggs, C. N. Mitchell, P. S. J. Spencer, P. Yin, and B. Zapfe (2007), Four-dimensional GPS imaging of space weather storms, *Space Weather*, *5*, S02003, doi:10.1029/2006SW000237.

Chau, J. L., and R. F. Woodman (2005), D and E region incoherent scatter radar density measurements over Jicamarca, *J. Geophys. Res.*, *110*, A12314, doi:10.1029/2005JA011438.

Daley, R. (1991), *Atmospheric Data Analysis*, Cambridge Univ. Press, New York.

Daley, R., and E. Barker (2000), The NAVDIS source book 2000: NRL atmospheric variational data assimilation system, *Tech. Rep. NRL Publ. NRL/PU/7530-00-418*, Naval Res. Lab., Monterey, Calif.

Dyrud, L. P., E. Kudeki, and M. Oppenheim (2007), Modeling long duration meteor trails, *J. Geophys. Res.*, *112*, A12307, doi:10.1029/2007JA012692.

Fesen, C. G., G. Crowley, R. G. Roble, A. D. Richmond, and B. G. Fejer (2000), Simulation of the pre-reversal enhancement in the low latitude vertical ion drifts, *Geophys. Res. Lett.*, *27*(13), 1851–1854.

Forbes, J. M. (1981), The equatorial electrojet, *Rev. Geophys.*, *19*, 469–504.

Friedrich, M., and K. M. Torkar (2001), FIRI: A semiempirical model of the lower ionosphere, *J. Geophys. Res.*, *106*(A10), 21,409–21,418.

Friedrich, M., K. M. Torkar, G. A. Lehmacher, C. L. Croskey, J. D. Mitchell, E. Kudeki, and M. Milla (2006), Rocket and incoherent scatter radar common-volume electron measurements of the equatorial lower ionosphere, *Geophys. Res. Lett.*, *33*, L08807, doi:10.1029/2005GL024622.

Garcia-Fernandez, M., M. Hernandez-Pajares, M. Juan, and J. Sanz (2003), Improvement of ionospheric electron density estimation with GPSMET occultations using Abel inversion and VTEC information, *J. Geophys. Res.*, *108*(A9), 1338, doi:10.1029/2003JA009952.

Hajj, G. A., and L. J. Romans (1998), Ionospheric electron density profiles obtained with the Global Positioning System: Results from the GPS/MET experiment, *Radio Sci.*, *33*(1), 175–190.

Hajj, G. A., R. Ibanez-Meier, E. R. Kursinski, and L. J. Romans (1994), Imaging the ionosphere with the Global Positioning System, *Int. J. Imaging Syst. Technol.*, *5*, 174–184.

Hajj, G. A., L. C. Lee, X. Pi, L. J. Romans, W. S. Schreiner, P. R. Straus, and C. Wang (2000), COSMIC GPS ionospheric sensing and space weather, *Terr. Atmos. Oceanic Sci.*, *11*(1), 235–272.

Hajj, G. A., E. R. Kursinski, L. J. Romans, W. I. Bertiger, and S. S. Leroy (2002), A technical description of atmospheric sounding by GPS occultation, *J. Atmos. Sol. Terr. Phys.*, *64*, 451–469.

Hernandez-Pajares, M., J. M. Juan, and J. Sanz (2000), Improving the Abel inversion by adding ground GPS data to LEO radio occultations in ionospheric sounding, *Geophys. Res. Lett.*, *27*, 2473–2476.

Hysell, D. L. (2007), Inverting ionospheric radio occultation measurements using maximum entropy, *Radio Sci.*, *42*, RS4022, doi:10.1029/2007RS003635.

Hysell, D. L., and J. L. Chau (2001), Inferring E region electron density profiles at Jicamarca from Faraday rotation of coherent scatter, *J. Geophys. Res.*, *106*(A12), 30,371–30,380.

Hysell, D. L., and E. Kudeki (2004), Collisional shear instability in the equatorial F region ionosphere, *J. Geophys. Res.*, *109*, A11301, doi:10.1029/2004JA010636.

Jakowski, N., A. Wehrenpfennig, S. Heise, C. Reigber, H. Lühr, L. Grunwaldt, and T. K. Meehan (2002), GPS radio occultation measurements of the ionosphere from CHAMP: Early results, *Geophys. Res. Lett.*, *29*(10), 1457, doi:10.1029/2001GL014364.

Kelley, M. C., V. K. Wong, G. A. Hajj, and A. J. Mannucci (2004), On measuring the off-equatorial conductivity before and during convective ionospheric storms, *Geophys. Res. Lett.*, *31*, L17805, doi:10.1029/2004GL020423.

Kursinski, E. R., et al. (1996), Initial results of radio occultation observations of Earth's atmosphere using the Global Positioning System, *Science*, *271*, 1107–1110.

Lei, J., et al. (2007), Comparison of COSMIC ionospheric measurements with ground-based observations and model predictions: Preliminary results, *J. Geophys. Res.*, *112*, A07308, doi:10.1029/2006JA012240.

Liou, Y.-A., A. G. Pavelyev, S.-F. Liu, A. A. Pavelyev, N. Yen, C.-Y. Huang, and C.-J. Fong (2007), FORMOSAT-3/COSMIC GPS Radio Occultation Mission: Preliminary results, *IEEE Trans. Geosci. Remote Sens.*, *45*(11), 3813–3826, doi:10.1109/TGRS.2007.903365.

Martinis, C., J. V. Eccles, J. Baumgardner, J. Manzano, and M. Mendillo (2003), Latitude dependence of zonal plasma drifts obtained from dual-site airglow observations, *J. Geophys. Res.*, *108*(A3), 1129, doi:10.1029/2002JA009462.

Mayer, C., and N. Jakowski (2009), Enhanced *E*-layer ionization in the auroral zones observed by radio occultation measurements onboard CHAMP and Formosat-3/COSMIC, *Ann. Geophys.*, *27*, 1207–1212.

Phinney, R. A., and D. L. Anderson (1968), On the radio occultation technique for studying planetary atmospheres, *J. Geophys. Res.*, *73*(5), 1819–1827.

Reinisch, B. W. (1986), New techniques in ground-based ionospheric sounding and studies, *Radio Sci.*, *21*, 331–341.

Roble, R. G., and E. C. Ridley (1994), A thermosphere-ionosphere mesosphere electrodynamics general circulation model (time-GCM): Equinox solar minimun simulations (30–500 km), *Geophys. Res. Lett.*, *21*, 417–420.

Schreiner, W. S., S. V. Sokolovskiy, C. Rocken, and D. C. Hunt (1999), Analysis and validation of GPS/MET radio occultation data in the ionosphere, *Radio Sci.*, *34*(4), 949–966.

Shume, E. B., D. L. Hysell, and J. L. Chau (2005a), Electron density profiles in the equatorial E region ionosphere derived from a bistatic coherent scatter radar experiment in Peru, *Geophys. Res. Lett.*, *32*, L01107, doi:10.1029/2004GL021715.

Shume, E. B., D. L. Hysell, and J. L. Chau (2005b), Zonal wind velocity profiles in the equatorial electrojet derived from phase velocities of type II radar echoes, *J. Geophys. Res.*, *110*, A12308, doi:10.1029/2005JA011210.

Straus, P. R. (1999), Correcting GPS occultation measurements for ionospheric horizontal gradients, in *Proceedings of the Ionospheric Effects Symposium*, edited by J. M. Goodman, pp. 700–709, Off. of Nav. Res., Washington, D. C.

Sultan, P. J. (1996), Linear theory and modeling of the Rayleigh-Taylor instability leading to the occurrence of equatorial spread *F*, *J. Geophys. Res.*, *101*(A12), 26,875–26,891.

Syndergaard, S. (2002), A new algorithm for retrieving GPS radio occultation total electron content, *Geophys. Res. Lett.*, *29*(16), 1808, doi:10.1029/2001GL014478.

Tsai, L.-C., and W.-H. Tsai (2004), Improvement of GPS/MET ionospheric profiling and validation using Chung-Li ionosonde measurements and the IRI model, *Terr. Atmos. Oceanic Sci.*, *15*, 589–607.

Tsunoda, R. T. (2006), Day-to-day variability in equatorial spread F: Is there some physics missing?, *Geophys. Res. Lett.*, *33*, L16106, doi:10.1029/2006GL025956.

Wu, B.-H., V. Chu, P. Chen, and T. Ting (2005a), FORMOSAT-3/COSMIC science mission update, *GPS Solutions*, *9*, 111–121, doi:10.1007/s10291-005-0140-z.

Wu, D. L., C. O. Ao, G. A. Hajj, M. de la Torre Juarez, and A. J. Mannucci (2005b), Sporadic *E* morphology from GPS-CHAMP radio occultation, *J. Geophys. Res.*, *110*, A01306, doi:10.1029/2004JA010701.

Wu, X., X. Hu, X. Gong, X. Zhang, and X. Wang (2009a), Analysis of the inversion error of ionospheric occultation, *GPS Solutions*, *13*, 231–239, doi:10.1007/s10291-008-0116-x.

Wu, X., X. Hu, X. Gong, X. Zhang, and X. Wang (2009b), An asymmetry correction method for ionospheric radio occultation, *J. Geophys. Res.*, *114*, A03304, doi:10.1029/2008JA013025.

Wu, X. C., X. Hu, and X. Y. Gong (2008), Three dimensional model constrained inversion method for ionospheric occultation (in Chinese), *Chin. J. Geophys.*, *51*(3), 618–625.

Zalesak, S. T., and S. L. Ossakow (1982), On the prospects for artificially inducing equatorial spread *F*, *Tech. Rep. Memo. Rep. 4899*, Naval Res. Lab., Washington, D. C.

G. S. Bust and F. S. Rodrigues, Atmospheric & Space Technology Research Associates, 12703 Spectrum Drive, Suite 101, San Antonio, TX 78249, USA. (gbust@astraspace.net; frodrigues@astraspace.net)

J. L. Chau, Radio Observatorio de Jicamarca, Apartado 13-0207, Lima 13, Peru. (jchau@jro.igp.gob.pe)

M. J. Nicolls, Center for Geospace Studies, SRI International, 333 Ravenswood Avenue, Menlo Park, CA 94025, USA. (michael.nicolls@sri.com)